

# Jitter Correction Algorithms for the *COROT* Satellite Mission: Validation with Test Bench Data and *MOST* On-Orbit Photometry

F. DE OLIVEIRA FIALHO, V. LAPEYRERE, AND M. AUVERGNE

Laboratoire d'Etudes Spatiales et d'Instrumentation en Astrophysique, Observatoire de Paris-Meudon, Meudon, France; fabio.fialho@obspm.fr

R. DRUMMOND, B. VANDENBUSSCHE, AND C. AERTS

Instituut voor Sterrenkunde, Katholieke Universiteit Leuven, Leuven, Belgium

AND

R. KUSCHNIG AND J. M. MATTHEWS

Department of Physics and Astronomy, University of British Columbia, Vancouver, Canada

Received 2006 November 13; accepted 2007 February 13; published 2007 March 8

**ABSTRACT.** We demonstrate the effectiveness and robustness of photometric correction algorithms for satellite pointing jitter in the upcoming space mission *COROT*, which will study asteroseismology and search for exoplanets. Two algorithms based on model-based estimation and decorrelation are tested in two ways: (1) with artificial light sources in the *COROT* CCD test bench, and (2) with on-orbit photometry from the Canadian *MOST* (*Microvariability and Oscillations of Stars*) satellite. Both algorithms effectively correct for pointing jitter to yield the expected results based on the inputs. The test with *MOST* data on a multiperiodic pulsating star demonstrates that the model-based estimation method recovers the oscillation signals better, while the decorrelation technique is more reliable if a poor model of the point-spread function is applied to the data. Therefore, the two algorithms complement one another and should both be applied to *COROT* photometry.

## 1. INTRODUCTION

*COROT* is a high-precision photometry mission for asteroseismology and the search for exoplanets (Baglin & the *COROT* Team 1998). It was launched in 2006 December to conduct long-duration observations. *COROT* is based on optimized fixed-aperture photometry, which means that only a total stellar flux within a mask will be downloaded.

Jitter is the lack of stability of the attitude control system (ACS). This small motion of the satellite's line of sight pollutes the photometric signal because of flat-field and edge effects. The flat-field effect is due to variation in quantum efficiency between pixels. The edge effect is due to the photometric aperture (mask). If the mask is fixed at the CCD level and the observed star is in its center, then satellite motion moves flux out of the mask, decreasing the measured integrated flux.

Even if these effects provoked by the ACS had been taken into account during the design phase, they would cause non-negligible pollution in the photometry, creating undesirable noise. Thus, as an important step in the *COROT* reduction pipeline, all observed stars must pass through jitter correction in order to eliminate and/or ensure that no relevant jitter harmonics are present in the reduced data. Two algorithms were developed to correct for the jitter effect and were explained in Drummond et al. (2006, hereafter Paper I) and tested on simulated data.

A test bench was mounted in Paris Observatory (LESIA, Meudon site) to characterize the *COROT* flight CCDs, giving us an opportunity to generate star images as close as possible to what we expect from *COROT* in flight. In addition, *MOST*<sup>1</sup> (Walker et al. 2003), a stellar photometer similar to *COROT*, was launched in 2003, and close collaboration has allowed us to test the algorithms on in-orbit data. These data and tests have allowed us to evaluate the correction quality in preparation for the launch of *COROT*.

This paper therefore deals with the validation of jitter correction algorithms and the testing of their robustness, and is organized as follows: § 2 gives an overview of the methods tested; § 3 shows the *COROT* test bench data reduction and jitter validation; § 4 covers the *MOST* data reduction and jitter validation (the preservation of scientific information also is verified); and finally, § 5 draws conclusions from this work.

## 2. METHOD

We considered two different approaches to correct for flux loss due to jitter. This resulted in two distinct methods: a model-based estimation and a decorrelation correction. For the first

---

<sup>1</sup> *MOST* (*Microvariability and Oscillations of Stars*) is a Canadian Space Agency mission operated jointly by Dynacon, Inc., and the Universities of Toronto and British Columbia, with assistance from the University of Vienna.

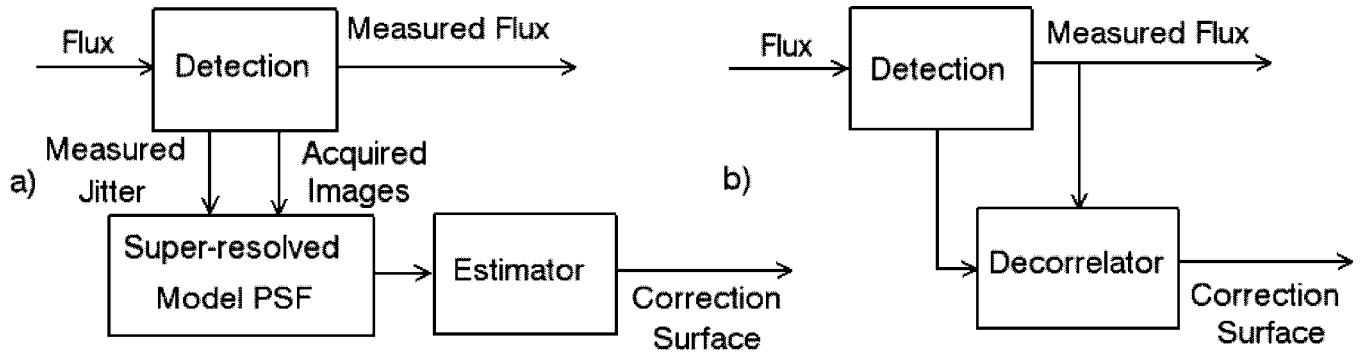


FIG. 1.—Photometric jitter correction using (a) model-based estimation and (b) decorrelation.

method, we assume that the process is well known. Consequently, we have an assemblage of star images that allows us to create a superresolved PSF (Pinheiro da Silva et al. 2006) that will be used to estimate the flux loss due to jitter. For the second method, we assume no knowledge of the process; we just have the inputs and outputs—a “black box” system. In the latter case, decorrelation is a reasonable approach to eliminating signal perturbations. Figure 1 shows these two approaches schematically.

In the first case, by knowing the perturbation (measured jitter) and the process model (PSF+photometric aperture), we can estimate flux losses and calculate the correction surface to be applied to the measured photometry. In the second case, with no knowledge about the detection process, two-dimensional decorrelation is calculated based on measured signals, providing the correction surface to be applied to the measured photometry. Once correction surfaces are computed, jitter correction can be performed as shown in Figure 2.

Using jitter data, we can look at the correction surface in order to define the gain that must be applied to the measured flux to correct it. We refer the reader to Paper I for the details on each method used. Simulations have been made to validate these methods and to evaluate their effectiveness. The most important conclusion was that both methods work well, but

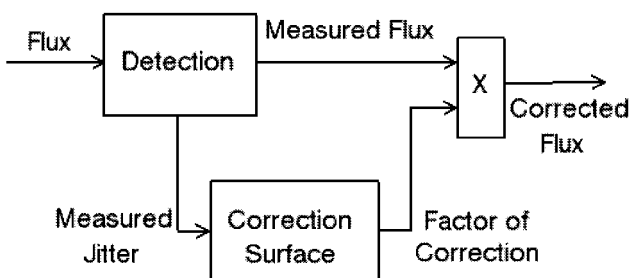


FIG. 2.—General scheme of the jitter photometric correction using a correction surface based on a superresolved PSF or decorrelation.

close care must be taken in their application, to ensure good quality results. This issue is addressed later in this paper.

The criteria adopted here to evaluate test bench and *MOST* corrections are not exactly the same as those used in Paper I. For the test bench data, there is no input scientific oscillation signal, and the actual pointing jitter does not contain high-frequency power. For the *MOST* data, the precision after data reduction was not high enough. In fact, the *MOST* data are an early case of direct imaging (secondary science) observations, and the resulting precision is therefore not at the level expected for *COROT* primary science photometry.

### 3. *COROT* TEST BENCH

The *COROT* test bench was developed to characterize the flight model CCDs. It consists of a CCD mounted inside a cryostat system, enabling us to maintain its pressure at about  $10^{-5}$  mbar and a temperature at  $-40^{\circ}\text{C}$ , with fluctuations of less than  $0.01^{\circ}\text{C}$ .

The optical configuration for the photometric test case is shown in Figure 3. Light is introduced into the sphere through the optic fiber, and a perforated plate creates a star field illuminated homogeneously at the exit of the sphere. Each of the light spots has a diameter of about 0.2 mm. For jitter tests, a white light-emitting diode (LED) is used. Jitter is created by moving the optics system using a servomechanism system. The photometric test that was performed was designed to evaluate the correction efficiency for high levels of jitter. Hence, we chose a 2 pixel peak-to-peak sine wave simulation with a 2 minute period ( $f_0 = 8.33$  mHz) in both axes, to avoid low-frequency test bench noise. For further information about the *COROT* test bench, see Lapeyrere et al. (2006).

#### 3.1. *COROT* Test Bench Data Reduction

The test bench provides digitized images containing background and offset windows and observed stars in ADUs (analog-to-digital units). Our goal at this stage is to perform aperture photometry. In order to achieve this, we must calculate

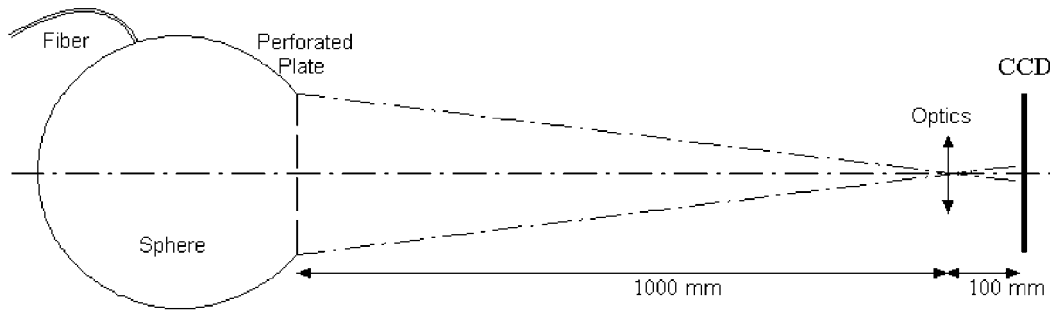


FIG. 3.—Optics for aperture photometry on the *COROT* test bench.

pointing errors, the superresolved PSF, the aperture, and the integrated flux. Figure 4 is a block diagram showing all the necessary steps.

This is a version of space-based aperture photometry that has been adapted to fit our data needs. The offset is considered as part of the background block, and the superresolved PSF (Pinheiro da Silva et al. 2006) is calculated instead of the 1 pixel resolution PSF. This last step is necessary in order to achieve the required *COROT* performance.

The CCD offset is a more significant source of noise for the test bench than it will be for *COROT*. This is due to contamination by test bench electronic noise and a coupling between the servomechanism and the electronic system. Thus, offset noise pollutes many frequencies in the spectrum. A simple way to correct this is to use the average offset. To check if the correction is done well, we must use the whole star window instead of the mask, to avoid edge effects due to jitter. Figure 5 shows the Fourier spectrum of complete star window photometry after background and offset corrections.

Only one contaminated frequency remains, corresponding to the fundamental jitter frequency  $f_0$  (2 minutes, or 8.33 mHz). This residual frequency is not due to interference between the servomechanism and the electronic system, but to a flat-fielding effect. It is important to keep in mind that flat-field noise in the photometry will be negligible in mission conditions, because the satellite jitter spectrum has a different power distribution than that generated here.

We had initially chosen to generate jitter with a 2 minute period. However, nonlinearities in the test bench forced us to

create slightly different pointing errors. This is due to temperature changes that cause the CCD to move slightly. Figure 6 shows the pointing errors computed in the “image centroids” block (Fig. 4), along with their Fourier spectra. The spectra show a line at  $f_0$  (2 minute period) as expected, but some power appears around 1.55 mHz for the y-displacements, due to the problem of temperature described above, which will have an impact on photometry, as we see later in Figure 9.

The superresolved PSF is calculated based on pointing errors and star images corrected for background and offset. Figure 7 shows the result. This PSF allows us to calculate the photometric aperture based on signal-to-noise ratio (S/N) optimization, shown in Figure 8. The algorithm used here is a simplified version of the method developed specifically to match *COROT* requirements. Howell (1989) provides a good example of the principle of S/N optimization in aperture photometry.

As the last step of data reduction, we measure the flux within the aperture. Figure 9 shows the results.

Some important details are revealed by this Fourier spectrum, the most important of all being the high nonlinearity of the problem. Let us start with the most powerful harmonic, at 16.66 mHz (i.e., at  $2f_0$ ). Almost all power due to jitter noise is at this frequency. This is because of symmetry within the problem we are handling. In order to understand it, we can make a simplified, one-dimensional illustration of the jitter effect on photometry. Let us imagine that the PSF is nothing more than a semicircle, and the mask is just two barriers defining the left and right edges. The stellar flux is constant, and the only perturbation is the jitter that corresponds to a sine

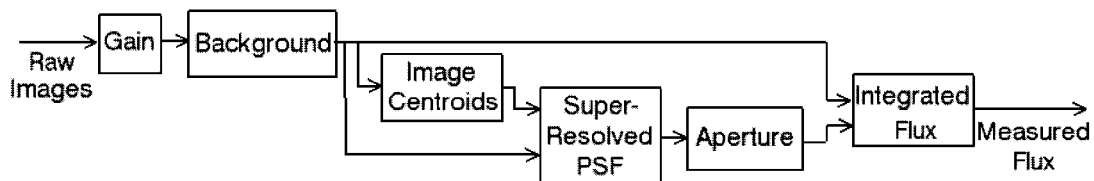


FIG. 4.—Block diagram of data reduction pipeline.

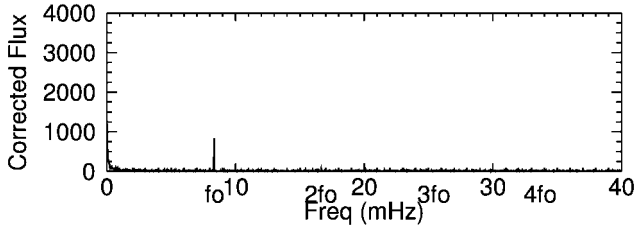


FIG. 5.—Fourier spectrum of complete star window photometry after background and offset corrections, in parts per million (ppm). The y-axis scale is extended to 4000 ppm to allow comparison with the aperture photometry of Fig. 9. The fundamental jitter frequency  $f_0$  (2 minute period jitter sine wave) and its multiples are indicated on the x-axis to simplify the identification of harmonics.

wave of period  $p$ , with amplitude varying between  $\pm dx$ . Due to symmetry, one period of jitter provokes two periods of oscillation on photometry; i.e., jitter signal in  $f_0$  generates jitter photometric noise in  $2f_0$ . Figure 10 illustrates this effect.

In reality, Figure 9 shows many frequencies other than  $f_0$ . It is clear that in the real world, the PSF and mask are not symmetric. Distortions in photometry are created, and this results in frequency combinations like the ones we see around the fundamental frequency. They are combinations of  $f_0$  and the frequencies around 1.55 mHz that we see in Figure 6d. We can also take advantage of this nonlinearity in the jitter signal to show how the test results extend to jitter at multiple frequencies and amplitudes. Due to symmetry and the nonlinear response of the problem explained above, the frequencies around 1.55 mHz will combine with the fundamental

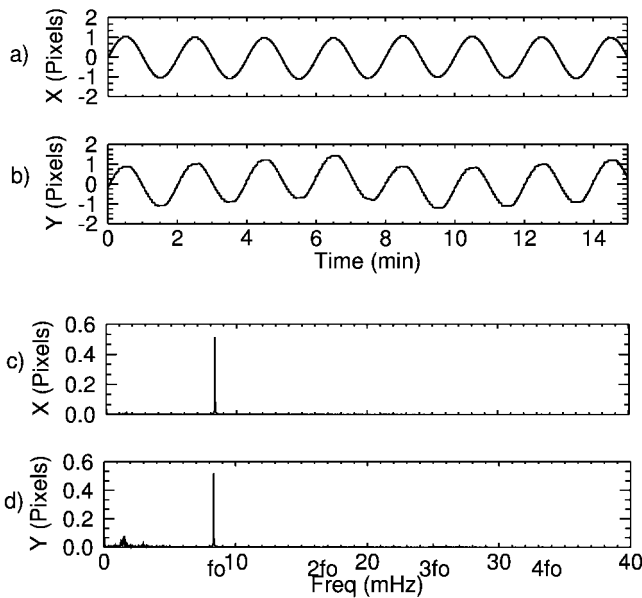


FIG. 6.—Pointing error in (a) x-axis and (b) y-axis, and their respective Fourier spectra in (c) and (d).

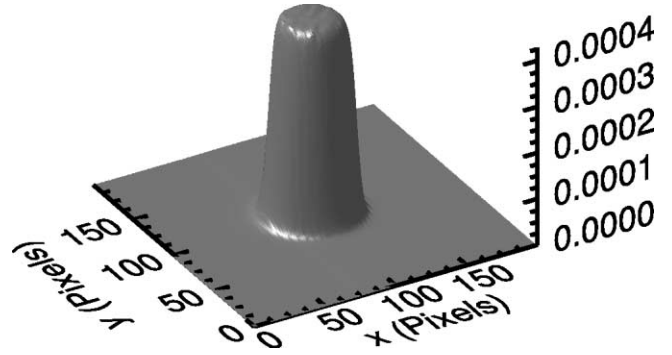


FIG. 7.—Normalized superresolved PSF. Resolution is 0.25 pixels.

frequency, provoking patterns in the photometry such as those we see repeated every  $2n \times f_0$ , as in the expanded area of Figure 9b.

The flat field remains the main source of noise at  $f_0$  when we compare Figures 9b and 5, another consequence of the symmetry explained above.

### 3.2. COROT Test Bench Jitter Correction Validation

All validations below are based on the block diagrams of Figures 1 and 2, and all the necessary data were produced as described in the section above. The first step of jitter correction is to calculate the correction surfaces. Figure 11 shows surfaces for both methods. Using these surfaces, we can perform the photometric correction of jitter that is shown in Figure 12.

If we visually compare the time-domain Figures 12a and

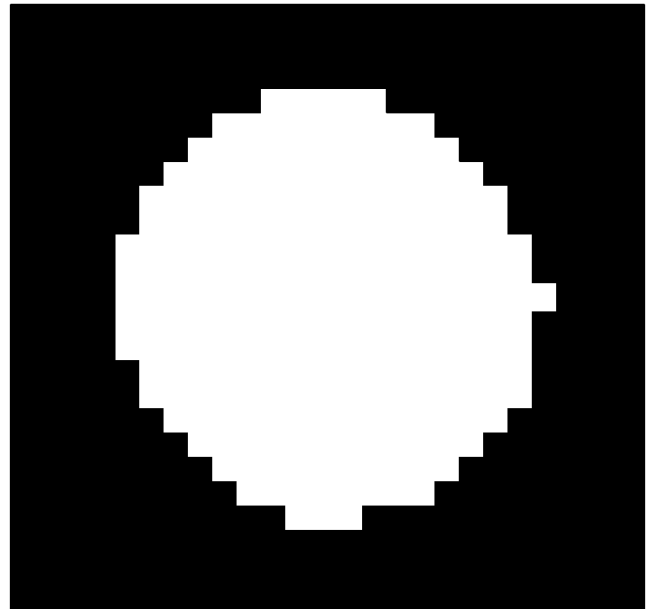


FIG. 8.—Image of 50 × 50 pixel photometric aperture. It has 269 pixels and a S/N of 2155.

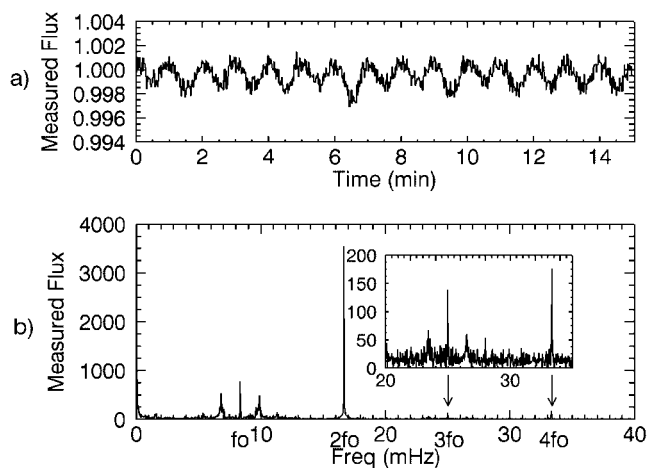


FIG. 9.—(a) Normalized aperture photometry of a star, and (b) its Fourier spectrum, in ppm.

12*b* to Figure 9*a*, we see that the flux is recovered very well, and the main noise is now essentially photon noise. Comparing Figure 12*c* (model-based correction) to Figure 9*b* (before correction), we can still see residual jitter at  $2f_0$ . This is expected, due to accuracy limitations of the model. In fact, it is impossible to have a perfect correction. However, by increasing model accuracy using a superresolved PSF, we ensure a sufficiently accurate correction for the seismology channel of the *COROT* satellite.

We also see that flat-field noise is still present at  $f_0$ . Model-based correction is not supposed to correct this. A pixel response nonuniformity map must also be used in order to correct this effect.

The decorrelation method (Fig. 12*d*) has corrected the flux for both types of jitter effect: flat field and edge. This demonstrates that decorrelation corrects for flux variations that are in phase with the barycenter displacement. If a stellar oscillation has the same frequency and is in phase with the satellite motion, it will be “corrected,” resulting in a loss of scientific signal. If it is out of phase, then we will see a peak in the power spectrum at the jitter frequency, with an amplitude corresponding to the phase shift. Table 1 summarizes the result statistics. The corrections made using a model-based estimation or decorrelation produce similar results, as was verified graphically. The difference in the S/N comes from flat-field correction with the decorrelation method. The difference in S/N with respect to the ideal case of only photon noise comes from residuals in offset and background correction.

Since this test used 2 pixel peak-to-peak displacement, this validation assures us of jitter correction precision even if the ACS degrades.

#### 4. MOST DATA

We continue on to data coming from the *MOST* satellite. Before talking about the treatment of data, let us highlight the

technical similarities that allow us to use these data to validate algorithms developed for *COROT*. Table 2 summarizes the main characteristics for the *MOST* and *COROT* instruments, as far as this paper is concerned.

Both instruments are based on back-illuminated e2v CCDs working in Advanced Inverted Mode Operation (AIMO) and at the same operating temperature. Moreover, they work in low-Earth orbit, with about the same orbital period. Both instruments work with defocused images. All these similarities clearly show us how precious *MOST* knowledge, acquired from the *MOST* team and from analyzing *MOST* data, is for improving the quality of the *COROT* data reduction pipeline. As these satellites have some differences in on-board processing, the data available at ground level are not the same.

*MOST* downloads multipixel images, whereas *COROT* will carry out fixed-aperture photometry. So in the case of photometric correction of jitter, the images (proceeding from the open field [Walker et al. 2003]) that are downloaded by *MOST* can be treated at ground level and used to perform fixed-aperture photometry, which allows us to apply the *COROT* corrections and to validate them.

In order to do that, the same exercise undertaken with test bench images was carried out with a star observed by *MOST*, HD 61199 ( $m_v = 8.2$ ). This star was a secondary target during *MOST*’s first primary science observations (of Procyon) in early 2004. HD 61199 was discovered to be a multiperiodic  $\delta$  Scuti star, based on these data (Matthews et al. 2004). At this early stage in the *MOST* mission, the pointing performance of the satellite was within its scientific requirements but still had substantial pixel-to-pixel jitter. Later in the mission, the ACS performance was greatly improved to achieve pointing errors of only about  $\pm 1''$  (about 0.3 pixel). Therefore, these early *MOST* CCD images are particularly interesting for our jitter validation tests, since the jitter is relatively large and we can observe whether our jitter correction has affected the seismology signal in HD 61199.

#### 4.1. HD 61199 Data Reduction

The data reduction steps performed for *MOST* and for the test bench images are essentially the same. Despite special treatment for some *MOST* blocks, the discussion in this section is based on the steps shown in Figure 4, as they were followed for test bench data as well.

Data used in this test refer to day 1482 to 1492 of observations in *MOST* Julian Dates, using an exposure time of 30 s. The exposure time for these data was set by the very bright Fabry target Procyon, and was not optimized for HD 61199, provoking low S/N. Much higher S/N values can be obtained if longer exposure times are used for fainter targets like this. The data correspond to  $16 \times 16$  pixel star windows. No background windows are used because they are not acquired in the open field by *MOST*, in contrast to the *COROT* test bench. Unlike *COROT* test bench data, the main noise sources in *MOST* raw images are cosmic impacts and stray light var-

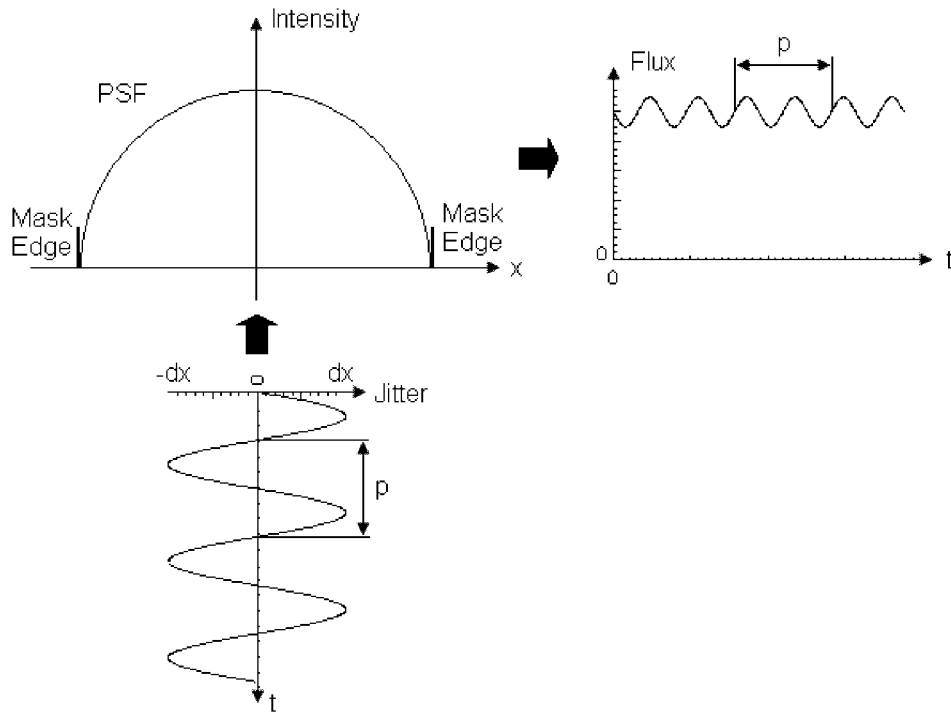


FIG. 10.—Illustration of the jitter effect on the photometry.

iation from scattered Earthshine. These two pollutants are filtered here in a simplistic way. The reader can find more precise *MOST* data reduction procedures in Rowe et al. (2006).

We begin with background correction. Background is hard to model because of the nonlinear stray light variation, and consequently, residuals are high. Figure 13 shows the amplitude spectra of complete window photometry before and after background subtraction. In Figure 13*b*, we also see many harmonics spread around the basic harmonics of scattered Earthshine (orbital frequency  $f_0$  and its multiples). This has three origins: the

residual background, the residual cosmic impacts, and the linear interpolation of missing points. Based on these images corrected for background, the image centroids block produces measured barycenter variations as shown in Figure 14.

The maximum acceptable pointing error has been limited to  $\pm 1$  pixel. Variations greater than this have been rejected, because the PSF and photometric aperture are too small in that case. Indeed, if a star moves more than 1 pixel, total flux loss on the edge of the mask is extremely high (more than 30%), which is not reasonable for the validation goals of this paper.

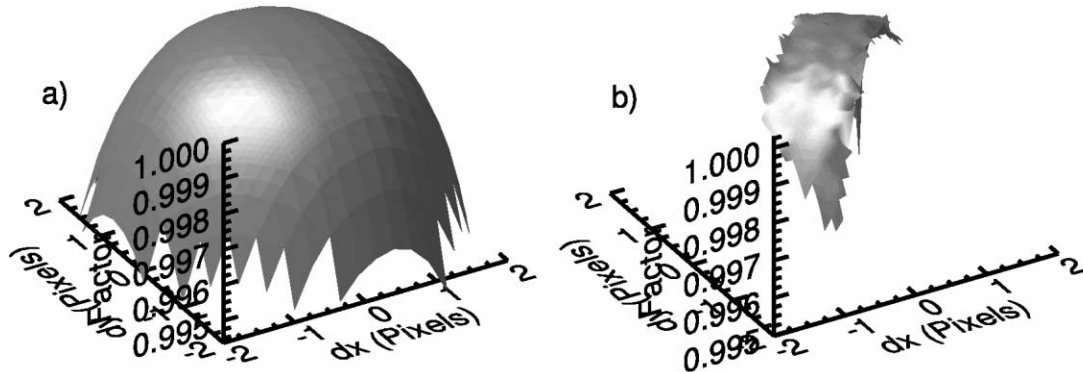


FIG. 11.—Correction surfaces based on (a) superresolved PSF and (b) decorrelation. Grid resolutions are 0.25 and 0.1 pixels, respectively. Grid resolution could in principle be increased for (b) decorrelation, but this would require more photometric measurements in order to achieve acceptable precision for each point of the surface.

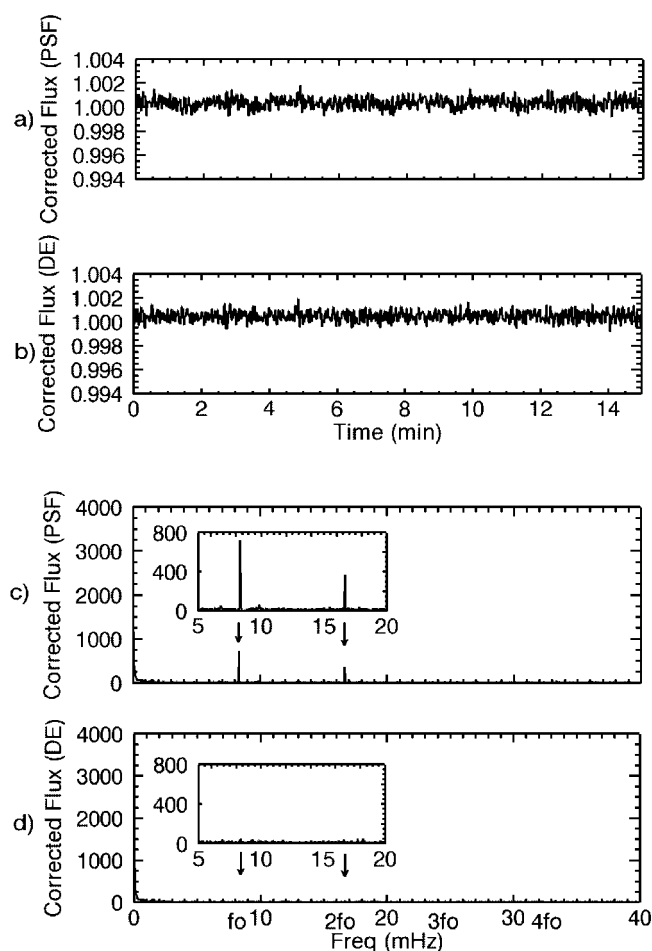


FIG. 12.—Normalized aperture photometry corrected for jitter using (a) model-based estimation and (b) decorrelation, with Fourier spectra given in ppm in (c) and (d), respectively.

With images corrected for background and pointing error measurements, we calculate the superresolved PSF for HD 61199 (Fig. 15). Compared to a typical *COROT* model PSF (Fig. 7), HD 61199's PSF is smaller in terms of number of pixels. The *COROT* PSF covers some 300 pixels, compared to about 20 for HD 61199, which greatly increases the sensitivity of the latter to jitter variations. For example, a 1 pixel shift of the *MOST* PSF can cause flux loss of about 30%, whereas *COROT* flux loss is about 2%. This is a consequence of de-

TABLE 1

JITTER PHOTOMETRIC CORRECTION STATISTICS FOR A TEST BENCH STAR DATA SET VERSUS AN IDEAL CASE WITH ONLY PHOTON NOISE

Result	Mean	Standard Deviation	S/N
Measured .....	0.99889	0.00087	1144.5
Corrected (PSF) .....	0.99973	0.00043	2302.2
Corrected (decorrelation) .....	0.99988	0.00042	2392.2
Ideal case .....	1	0.00036	2754.4

TABLE 2  
MAIN TECHNICAL CHARACTERISTICS OF *MOST* AND *COROT*  
CONCERNING APERTURE PHOTOMETRY ON THE  
ASTEROSEISMOLOGY CHANNEL

Characteristics	<i>MOST</i>	<i>COROT</i>
Main targets (mag) .....	6–12.5	5.4–9
Orbital period (minutes) .....	101.4	103
Altitude (km) .....	820	896
Time baseline (days) .....	60	150
Resolution ( $\mu$ Hz) .....	0.2	0.1
CCD .....	e2v 47-20	e2v 42-80
CCD temperature ( $^{\circ}$ C) .....	$-40 \pm 0.01$	$-40 \pm 0.01$
Sampling time (s) .....	30 <sup>a</sup>	1
Frequency range (mHz) .....	0.093–1	0.093–16.7
Jitter noise (pixels rms) .....	$\pm 0.33$	$\pm 0.22$

NOTE.—This information was taken from Walker et al. (2003) and Auvergne et al. (2003).

<sup>a</sup> For data used in this paper, 30 images with 1 s exposures each are summed to produce each 30 s image.

focused *COROT* imaging, whereas *MOST* images are in focus and unresolved. The photometric aperture consequently has no more than 10 pixels, as shown in Figure 16.

Aperture photometry is calculated based on the mask shown above and the images corrected for background. Figure 17 shows the results. We can see how sensitive the photometry is to jitter (i.e., to edge effects from the mask). A 1 pixel variation in satellite pointing produces a flux loss of more than 30% and high distortion in the time-series flux, as seen in Figure 17a. The Fourier spectrum of measured flux is completely polluted, as seen in Figure 17b, and the scientific information (multi-periodic oscillations) is hidden inside the noise. We do not even find the harmonics seen in Figure 13b. The reason for this is the nonlinear character of the problem; i.e., a nonsymmetrical mask and PSF that produce frequencies other than those present

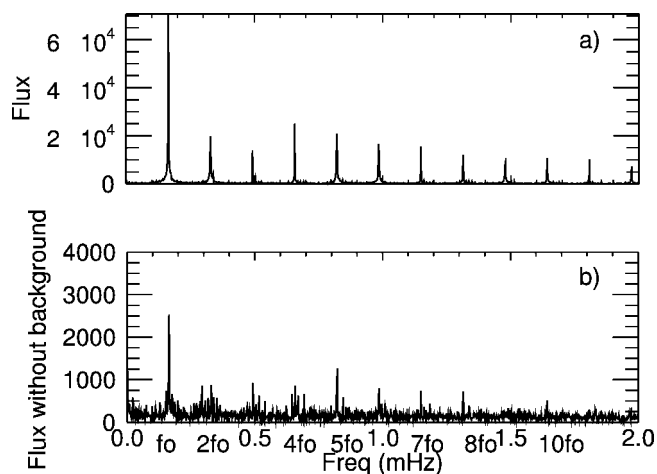


FIG. 13.—Fourier spectra of complete star window photometry (a) before and (b) after background subtraction, in ppm. Note that even after background subtraction, many frequencies are still contaminated by scattered earthshine.

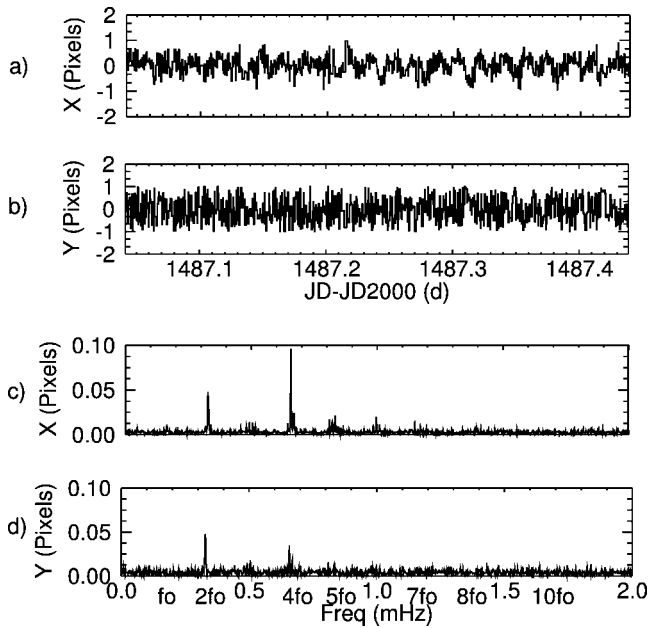


FIG. 14.—*MOST* pointing error in (a) *x*-axis and (b) *y*-axis in the CCD frame, and their respective Fourier spectra in (c) and (d). Note the existence of many harmonics. The two most important and higher amplitude frequencies are at  $2f_0$  and  $4f_0$  (0.32 and 0.64 mHz).

in the jitter. The jitter correction must be able to recover the science signal and the residual background noise.

#### 4.2. HD 61199 Jitter Correction Validation

Let us now apply jitter correction algorithms. First, we calculate correction surfaces, the results of which are shown in Figure 18. Based on these surfaces, the results of jitter correction are as shown in Figure 19. Table 3 shows the gain in S/N. Comparing Figure 17 (before correction) and Figure 19, we can see that the time-domain photometry is well corrected.

Matthews et al. (2004) find the main pulsation frequency is

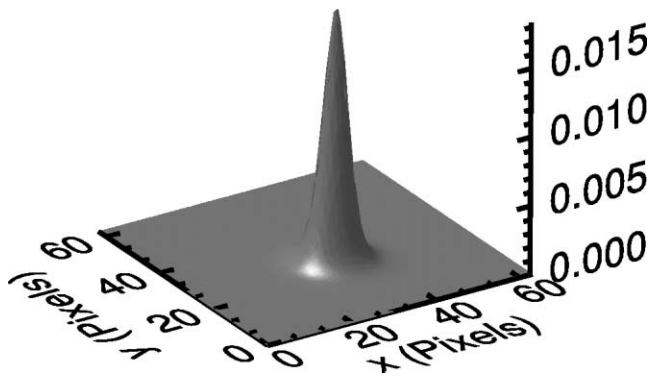


FIG. 15.—Normalized superresolved PSF of HD 61199. Resolution is 0.25 pixels.

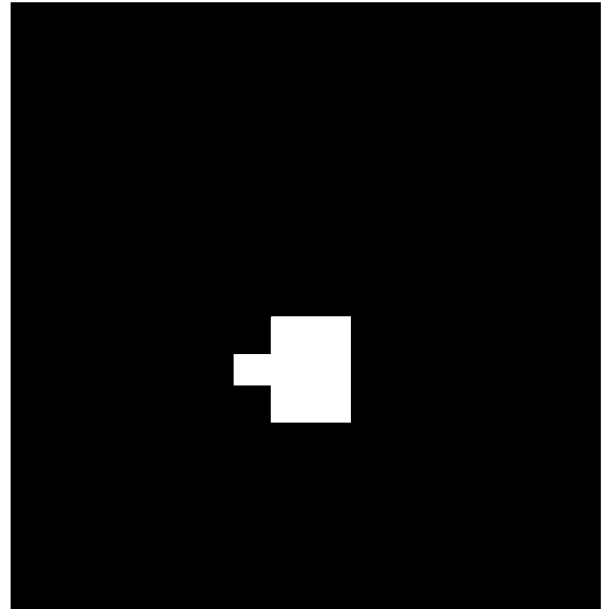


FIG. 16.—Image of  $16 \times 16$  pixel photometric aperture for HD 61199. It has 10 pixels and a S/N of 198.6.

at 0.292 mHz (57 minutes), which is exactly what we find in Figure 19c and 19d. The frequency spectra show that the oscillation frequency of the star has been preserved in both methods and that residual jitter noise is negligible compared to background noise.

Table 3 shows a gain greater than a factor of 6 in the S/N for both methods. The difference in the S/N between the ideal case with photon noise and the corrected flux is due to the residual scattered Earthshine.

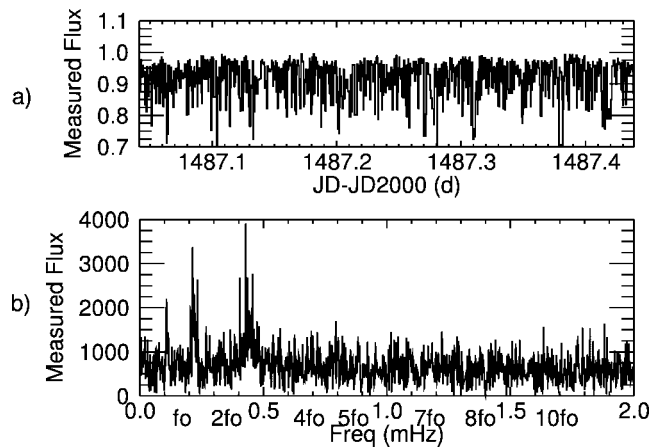


FIG. 17.—(a) Normalized aperture photometry of HD 61199, and (b) its Fourier spectrum, in ppm. In (a) the normalization is made based on the expected mean flux inside the mask when there is no jitter.

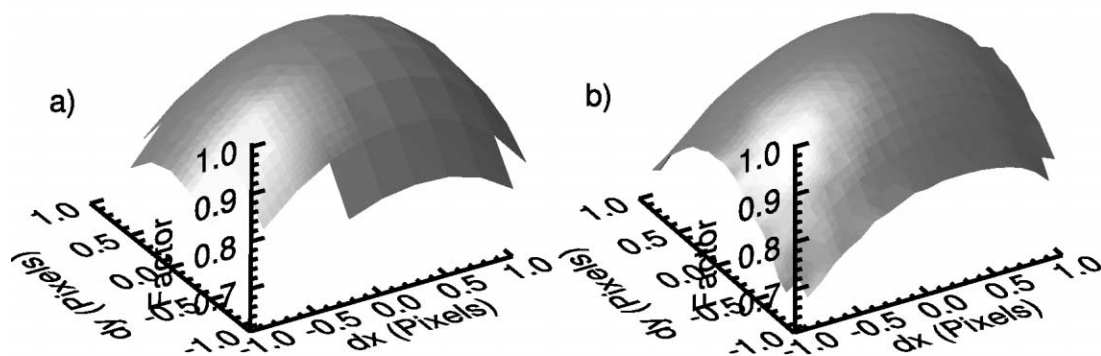


Fig. 18.—Correction surfaces for HD 61199 based on (a) superresolved PSF and (b) decorrelation. Grid resolutions are 0.25 and 0.1 pixels, respectively.

## 5. CONCLUSION

In this paper, we have explored the validation of two methods of photometric correction of jitter. The test bench allowed us to create images as close to expected in-flight *COROT* images as possible. A very good superresolved model PSF can be created from 1000 images and allows excellent model-based estimation correction. This method may leave some residuals, due to limitations in the accuracy of the model PSF, and flat-field effects. For good decorrelation, we need on the order of  $10^5$  photometric points. This method corrects for flat-field effects as well as the edge effect, but may reduce scientific signal, depending on its frequency and phase. Care should be taken if the expected scientific frequencies overlap with the jitter frequencies, in order to ensure an effective correction.

The availability of *MOST* on-orbit data was a valuable practical test of the algorithms. The *MOST* direct imaging PSF (which was set for that mission by the requirements for guide stars in the *MOST* focal plane, and was never originally intended for primary science) is narrower than the *COROT* PSF. The mask we assigned in this test is much smaller than the masks that will be used for *COROT*. This leads to high flux loss, even when jitter is restricted to 1 pixel variation (higher than that obtained in the *MOST* mission direct imaging reduction process); but this provides an even more rigorous test. A flux loss of about 30% is recovered by our jitter correction algorithms. This is all the more encouraging, considering that we have not tried to correct for other known instrumental and environmental effects in the *MOST* data (Reegen et al. 2006).

Since the test data come from a real star and not synthetic

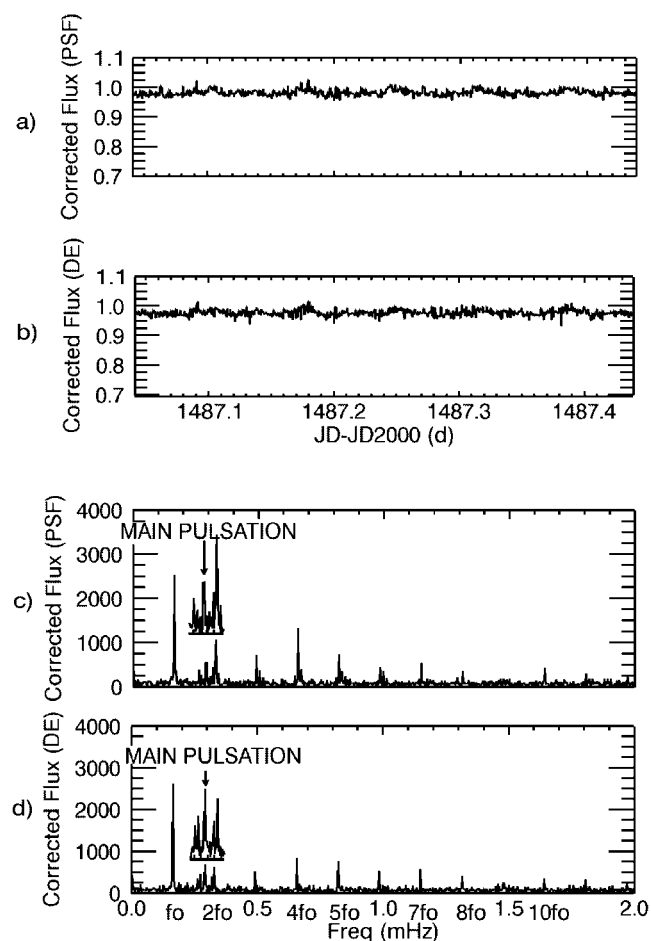


Fig. 19.—Normalized aperture photometry of HD 61199 corrected for jitter using (a) model-based estimation and (b) decorrelation, with Fourier spectra in ppm given in (c) and (d), respectively. Compare to Fig. 17.

TABLE 3

JITTER PHOTOMETRIC CORRECTION STATISTICS FOR HD 61199 VERSUS AN IDEAL CASE WITH ONLY PHOTON NOISE

Results	Mean	Standard Deviation	S/N
Measured .....	0.900	0.061	14.8
Corrected (PSF) .....	0.969	0.011	88.7
Corrected (decorrelation) .....	0.964	0.011	91.5
Ideal case .....	1	0.004	246.7

input, we cannot be absolutely certain of the frequency content of the intrinsic input signal. However, we recover the main pulsation period of HD 61199 at the same value (about 57 minutes) as that found in the independent analysis by the *MOST* mission team (Matthews et al. 2004). This is a strong demonstration of the robustness of both jitter correction methods.

Finally, we emphasize that both methods provide a good correction for jitter, despite their differences. Their individual strengths make them complementary, and both should be applied to *COROT* data.

This work was prepared as a Brazilian and Belgian contribution to the *COROT* project. We thank Annie Baglin for her valuable comments. F. O. F. is funded by the Brazilian Ministry of Science and Technology (CNPq, under grant 200206/2003-0). R. D., B. V., and C. A. are financed through the PRODEX program of the Belgian Belspo office, under grant C90199 (*COROT* Mission Data Exploitation II), and the Research Council of Leuven University, under grant GOA/2003/04. J. M. M. is funded by a grant from the Natural Sciences and Engineering Research Council (NSERC), Canada, and R. K. is supported by the Canadian Space Agency.

## REFERENCES

- Auvergne, M. et al. 2003, *Proc. SPIE*, 4854, 170  
 Baglin, A., and the *COROT* Team 1998, in *IAU Symp.* 185, *New Eyes to See Inside the Sun and Stars*, ed. F.-L. Deubner, J. Christensen-Dalsgaard, & D. W. Kurtz (Dordrecht: Kluwer), 301  
 Drummond, R., Vandebussche, B., Aerts, C., De Oliveira Fialho, F., & Auvergne, M. 2006, *PASP*, 118, 874 (Paper I)  
 Howell, S. B. 1989, *PASP*, 101, 616  
 Lapeyriere, V., Bernardi, P., Buey, J. T., Auvergne, M., & Tiphène, D. 2006, *MNRAS*, 365, 1171  
 Matthews, J. M., Kuschnig, R., Guenther, D. B., Walker, G. A. H., Moffat, A. F. J., Rucinski, S. M., Sasselov, D., & Weiss, W. W. 2004, *Nature*, 430, 51  
 Pinheiro da Silva, L., Auvergne, M., Toubanc, D., Rowe, J., Kuschnig, R., & Matthews, J. 2006, *A&A*, 452, 363  
 Reegen, P., et al. 2006, *MNRAS*, 367, 1417  
 Rowe, J. F., et al. 2006, *ApJ*, 646, 1241  
 Walker, G., et al. 2003, *PASP*, 115, 1023